First-order liquid-liquid phase transition in nitrogen-oxygen mixtures

Yang-Shun Lan,[1,2] Zhao-Qi Wang,[1,2] Lei Liu,[2] Guo-Jun Li,[1,2] Hua-Yang Sun,[3] Zhi-Jian Fu,[4] Yun-Jun Gu,[2] Guang Yang,[5] Lu-Ning Li,[5] Zhi-Guo Li,[2,*] Qi-Feng Chen,[2,†] and Xiang-Rong Chen[1,‡]

[1]*College of Physics, Sichuan University, Chengdu 610064, People's Republic of China*

[2]*National Key Laboratory for Shock Wave and Detonation Physics Research, Institute of Fluid Physics, Chinese Academy of Engineering Physics, Mianyang 621900, People's Republic of China*

[3]*Northwest Institute of Nuclear Technology, Xi'an 710024, People's Republic of China*

[4]*School of Electronic Information and Electrical Engineering, Chongqing University of Arts and Sciences, Chongqing 402160, People's Republic of China*

[5]*Science and Technology on Space Physics Laboratory, China Academy of Launch Vehicle Technology, Beijing 100076, People's Republic of China*

(Received 7 January 2021; revised 8 March 2021; accepted 6 April 2021; published 21 April 2021)

The first-order liquid-liquid phase transition (LLPT) describes the counterintuitive nature between two distinct liquids in a single system. However, the physical understanding of LLPT in simple liquid mixtures has remained elusive. Here, a first-order LLPT for nitrogen-oxygen (N-O) mixtures is investigated via extensive *ab initio* molecular dynamics simulations. The first-order LLPT is characterized by discontinuities of a short-range order and transport properties, occurring at the transition pressures identified by looking at isotherms. The LLPT in N-O mixtures is dominated primarily by the molecular-to-polymeric transformation. The resulting phase boundaries and further structural analysis show the crucial influence of oxygen on weakening the LLPT of N-O mixtures by promoting chemical reactions with nitrogen and crippling polymerizations. Furthermore, noncovalent interactions of short- to long-range van der Waals have evident impacts on the LLPT boundary. The introduction of the strongly constrained and appropriately normed functional with revised Vydrov–van Voorhis nonlocal correlation (SCAN-*r*VV10) functional to describe the phase-transition behaviors improves the agreement with experimental data. The results highlight the characteristic features of the complex interplay in binary mixtures and revisit the first-order phase transition of dense nitrogen.

DOI: 10.1103/PhysRevB.103.144105

I. INTRODUCTION

The first-order liquid-liquid phase transition (LLPT) is an unconventional transition between two liquid states in a single-component system, which has recently attracted considerable attention not only because of its counterintuitive nature but also as it is crucial to fundamentally understand the liquid state [1–3]. This transition has been found in some simple liquid systems such as silicon [4–6], sulfur [1], hydrogen [7–15], nitrogen [16,17], and carbon dioxide [18]. Accurate knowledge of the pivotal mechanisms for the phase transition in typical diatomic molecules above the melting temperature as well as the structural evolutions and critical temperatures in this medium is crucial to understand the internal structures and dynamics of planets in our solar system [9,19–21]. For hydrogen, molecular dissociation-induced LLPT under high pressures and temperatures (P-T) would suggest a density discontinuity within the interior of gas giant planets [9,10,12]. Nitrogen exhibits more complex behaviors under extreme P-T conditions, which forms a variety of polynitrogen molecules with a reduced bond order due to their ability to adopt differing bond types (single to triple) [16,17,22–24]. The phase diagrams are central for understanding how nitrogen behaves in the deep interiors of planets, where it can appear as a molecule due to ammonia dissociation [25]. This has stimulated strong research interest to probe the LLPT of nitrogen.

Enormous efforts have been made toward illustrating the polymerization effects and thermodynamic properties of liquid nitrogen. The chemical equilibrium model proposes the possibility of molecular-to-polymeric transformations to explain the second shock cooling of dynamic compression experiments [26,27]. The *ab initio* molecular dynamics (AIMD) simulations based on the Perdew-Burke-Erzenhof (PBE) functional [16] and the strongly constrained and appropriately normed (SCAN) meta-generalized gradient approximation (GGA) functional [17] proffer direct evidence for the first-order phase transition from molecular-to-polymeric fluid at pressures of 88 and 102 GPa at a temperature of 2000 K, respectively. Nevertheless, various experimental evidence, including Raman studies [28,29], synchrotron radiation x-ray diffraction measurements [30], and the latest laser heating observations [31], show that polymeric nitrogen emerges at higher pressures, and molecular nitrogen remains up to 116 GPa at 2080 K. The disagreements between theoretical and experimental results are likely due to the inappropriate

*zhiguo_li@foxmail.com
†chenqf01@gmail.com
‡xrchen@scu.edu.cn

treatment of noncovalent interactions between molecules in the exchange-correlation (XC) functional [9,17]. It has been demonstrated that the SCAN XC functional [17] with intermediate-range van der Waals (vdW) interactions can result in a larger transition pressure. Therefore, the predictive determination of the short- to long-range vdW for phase transitions in liquids requires accurate descriptions for different bond types under the effects of polymerization, which needs further exploration.

The LLPT of mixtures is more challenging than simple liquids due to the complex interactions between the system components [9,32–34]. Mazzola *et al.* performed quantum Monte Carlo (QMC) MD simulations on pure hydrogen and hydrogen-helium mixtures at a solar composition to show the crucial influence of helium on the first-order LLPT of hydrogen [9]. This strongly inspired exploring the effect of mixing on the LLPT of nitrogen. Here, we focus on a binary mixture of nitrogen and oxygen, which are the essential elemental components of detonation products and some gaseous planets [35–38]. To our knowledge, the first-order LLPT has not been found in liquid oxygen [39–43]. Moreover, distinct from hydrogen-helium mixtures, the participation of oxygen in nitrogen-oxygen (N-O) mixtures generates abundant chemical reactions and structural evolutions under high P-T conditions [9,22,44]. Overall, pure nitrogen liquid exhibits the first-order character and pure oxygen does not. However, the behavior of N-O mixtures under different N:O ratios remains unknown and is worthy of in-depth study.

In this paper, we perform extensive AIMD simulations to explore the potential first-order LLPT in N-O mixtures and revisit the LLPT of nitrogen under extreme thermobaric conditions. The SCAN functional with revised Vydrov-van Voorhis nonlocal correlation (SCAN-rVV10) functional was used to improve the short- to long-range vdW interaction descriptions in nitrogen and N-O mixtures. Various physical properties, including the equations of states (EOS), electronic conductivities, and liquid structures, were calculated to trace the LLPT of N-O mixtures. Moreover, four different mixing ratios were considered to investigate the effects of mixing on LLPT. Finally, we present a detailed structural analysis to determine the mechanism of LLPT in N-O mixtures and construct their LLPT boundaries. The work provides a comprehensive picture to understand the LLPT process in binary N-O mixtures under different N:O ratios.

II. COMPUTATIONAL METHODS

The AIMD simulations are implemented via the Vienna *ab initio* simulation package within the framework of the projected augmented-wave method [45,46]. Electronic exchange and correlation interactions are described by the PBE [47] functional and SCAN functional with revised Vydrov–van Voorhis nonlocal correlation (SCAN-rVV10) [48,49], respectively. The SCAN-rVV10 functional was used to include the long-range interactions of N-O mixtures while preserving the short- and intermediate-range description for SCAN [48]. The AIMD simulations are performed for a canonical ensemble (NVT) where the temperature, volume, and particle number in the cubic box are conserved quantities. Local thermodynamic equilibrium, i.e., equal electron and ion temperatures ($T = T_e = T_i$), are maintained through a Fermi-Dirac distribution at fixed T_e and Nosé-Hoover thermostats about T_i [50,51]. The Γ point is used to sample the Brillouin zone in all cases, and electronic wave functions are expanded with a plane-wave basis with an energy cutoff of 800 eV. Considering the crucial role of spin fluctuations in liquid oxygen before metallization occurs [43], the electron spin polarization is also deliberated in N-O mixtures. Four N-O systems are considered in this work (N:O=1:0, 4:1, 2:1, and 1:1). The cells containing 90–300 atoms are used to test the finite-size effects, as shown in Figs. S1 and S2 of the Supplemental Material (SM) [52]. It is found that the utilization of 90 atoms is sufficient for our work. The AIMD simulations run for at least 15 ps at each density-temperature (ρ-T) condition with a 1.0 fs ionic time step, and the total simulation time amounts up to 40 ps in the phase transition region. Moreover, the dynamic conductivity $\sigma(\omega)$ of each ρ-T condition is calculated via the Kubo-Greenwood formula [53–55] for 20 uncorrelated snapshots in the last 2 ps, where denser $3 \times 3 \times 3$ k points are set to sample the Brillouin zone. The dc electrical conductivity σ is given as the static limit of the dynamic conductivity. The rationality of this approach has been verified in previous works [56–58]. Detailed convergence tests are provided in the SM [52].

III. RESULTS AND DISCUSSION

The LLPTs of nitrogen and N-O mixtures are determined by tracing the discontinuity ($\partial P/\partial \rho \leqslant 0$) on the isotherms (see Fig. 1). A plateau is recognized on the pressure isotherms of liquid nitrogen below 4000 K, which confirms the diverging isothermal compressibility [$K_T \leqslant -V^{-1}(\partial V/\partial P)_T$] in this region. The 5000-K isotherm of liquid nitrogen does not show a plateau, which implies there is a critical temperature point (T_c) for LLPT between 4000 and 5000 K. From the inset of

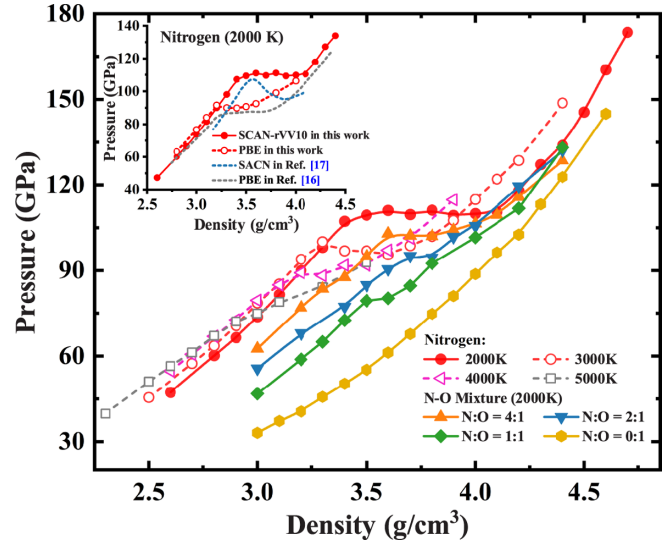

FIG. 1. Isothermal pressure-density curves of liquid nitrogen and N-O mixtures based on the SCAN-rVV10 functional. The plateaus on the isotherms indicate the existence of the first-order LLPT. Inset: Current liquid-nitrogen isotherm at 2000 K is compared with the previous SCAN [17] and PBE [16] simulation results.

Fig. 1, the AIMD simulations with different XC functionals show strong deviations on the transition pressure along the 2000-K isotherm of liquid nitrogen. The transition pressure from the present PBE functional is consistent with the calculated results from Boates *et al.* [16] within a 4% deviation. The transition pressure of the current SCAN-*r*VV10 functional is 109 GPa, which is larger than the simulation results from the PBE and SCAN functionals and reduces the disparity between experiments and theories [16,17,30,31]. The SCAN-*r*VV10 includes the short- to long-range vdW interactions and appears to be more suitable for the LLPT coexistence district. The participation of oxygen in N-O mixtures evidently affects the LLPT of the system. As the proportion of oxygen increases, the LLPT transition pressure of N-O mixtures is slightly lowered, as shown in Fig. 1. More importantly, the two-phase coexistence interval gradually narrows with an increasing oxygen ratio. The 2000-K isotherm of pure oxygen does not show any discontinuity and demonstrates that liquid oxygen has no first-order character at similar *P*-*T* conditions. At larger temperatures, the LLPT transition pressures decrease for N-O mixtures, as shown in Fig. S3 [52]. The signature of the LLPT disappears at high temperatures, and the critical temperatures T_c decrease at greater oxygen contents in N-O mixtures.

To gain insights into the nature of LLPT in N-O mixtures, the physical properties, including the equalization ratio ξ and the dc conductivity σ, are also examined and displayed in Fig. 2. Here, $\xi = \langle d_1 \rangle / \langle d_2 \rangle$ is defined as the ratio between the shortest d_1 and the second shortest d_2 interatomic distances [8,60]. This quantity reaches the limiting value of 1 in the polymeric fluid at high densities due to nearly the same d_1 and d_2 under polymeric states, and conversely tends to zero for molecular liquids under low-density conditions as d_1 fluctuates close to the equilibrium molecular bond length while d_2 represents the (large) intermolecular distance [8]. It is noted from Fig. 2(a) that ξ for nitrogen displays a noticeable jump, which occurs at the transition pressure as identified by looking at the 2000-K isotherm. When the molecular-to-polymeric transition of nitrogen occurs, the ξ of liquid nitrogen approaches 1 beyond the transition pressure. The inset of Fig. 2(a) shows that the neighbor length distribution correlations C_{NLDC} in LLPT are distributed in two regions with average distances of $d_1 \approx 1.09$ Å and $d_2 \approx 2.0$ Å and $d_1 \approx d_2 \approx 1.29$ Å, which correspond to the molecular [Fig. S5(a)] and polymeric [Fig. S5(b)] states, respectively [52]. Similar discontinuities occur in the N-O mixtures. However, the value of ξ decreases with the increase of oxygen ratio and reaches 0.65 for N:O = 1:1. Accordingly, the C_{NLDC} for N-O mixtures in Figs. S5(c)–S5(f) shows a new distribution area, which may indicate the formation of new molecular structures in N-O mixtures [52].

As confirmed by previous work, the liquid nitrogen undergoes a first-order phase transition to a polymeric liquid upon compression [16,61], which is connected with the simultaneous transition from the insulating liquid to a conducting fluid. Here, the conductive properties of N-O mixtures along the phase transition are investigated. As illustrated in Fig. 2(b), the dc conductivity σ of liquid nitrogen with the SCAN-*r*VV10 functional gradually increases from ~3 to ~100 S/cm before the phase transition, and then increases sharply to

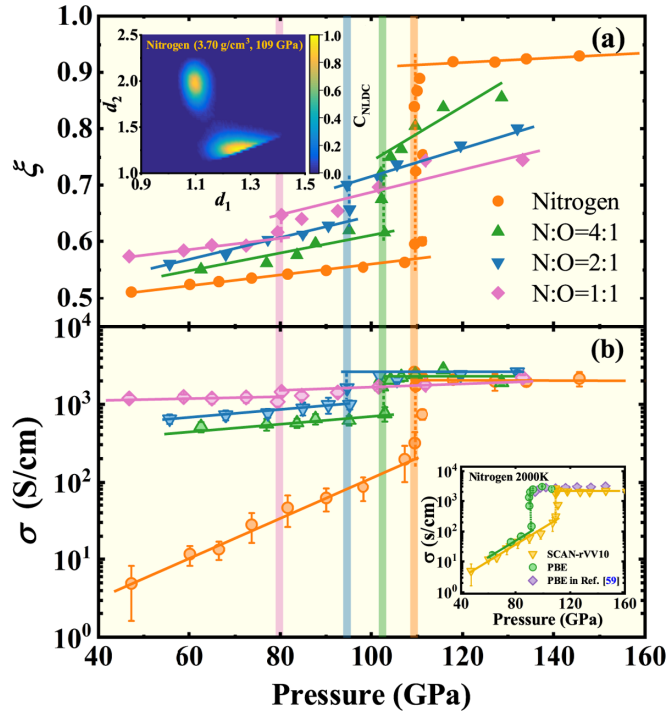

FIG. 2. The SCAN-*r*VV10 calculated (a) equalization ratio ξ and (b) dc conductivity σ along the 2000-K isotherms for liquid nitrogen and N-O mixtures. The lines are a guide to the eye, and the vertical bars indicate discontinuities of ξ and σ. Inset of (a): The confidence of neighbor length distribution correlations C_{NLDC} for the shortest length (d_1) and second shortest length (d_2) of neighboring atoms. Inset of (b): Comparison of isotherm of dc conductivity for liquid nitrogen at 2000 K derived from SCAN-*r*VV10 and PBE, respectively [59].

~1000 S/cm once the LLPT is complete. This feature is in agreement with the previous PBE calculations [59], except for the transition pressure, as shown in the inset of Fig. 2(b). The participation of oxygen significantly increases the conductivities of N-O mixtures at the low-density branch before the LLPT as oxygen contributes substantial electron mobilities within this regime [40,42,43]. This weakens the jump behavior of σ. It is noted that the σ of N-O mixtures is beyond 1000 S/cm after the LLPT, indicating the transition to a metallic state for the N-O mixture in the LLPT process. The discontinuities in the equalization ratio and dc conductivity are also captured by the PBE calculations in Fig. S6 [52].

The EOS, structure order parameters, and metallization transition have preliminarily revealed the physical characteristics of N-O mixtures in the LLPT process and the vital role of oxygen. To further explore the mechanism behind this, we examine the pair-correlation functions $g(r)$ of N-O mixtures. Figure 3 shows the calculated $g(r)$ of N-O mixtures at 3.3, 4.2, and 3.6–3.8 g/cm^3 on the 2000-K isotherms, which correspond to the states before, after, and in the LLPT, respectively. For pure nitrogen in Fig. 3(a), the molecular peak at 1.09 Å in the $g(r)_{\mathrm{N\text{-}N}}$ represents the triple bonded N_2 molecule, while the peak at 1.28 Å arises from the polymer networked by alternating single and double bonds. The evolution of $g(r)_{\mathrm{N\text{-}N}}$ definitely indicates the transformation from a molecular liquid

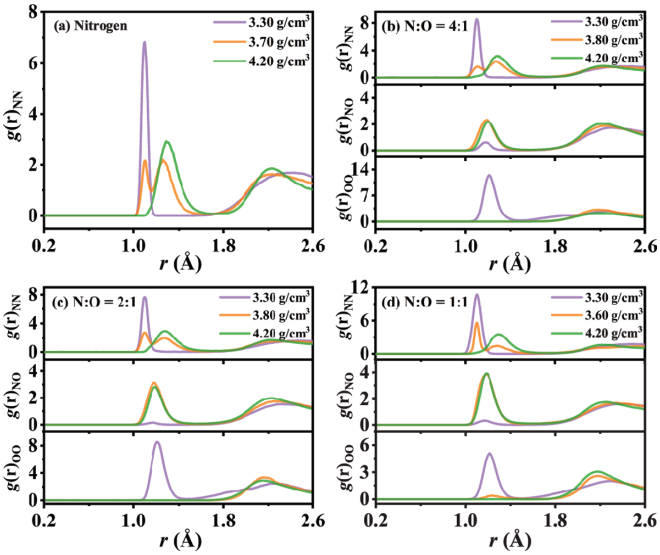

FIG. 3. Pair correlation functions $g(r)$ for N-N, N-O, and O-O of liquid N-O mixtures calculated using the SCAN-*r*VV10 functional at 2000 K.

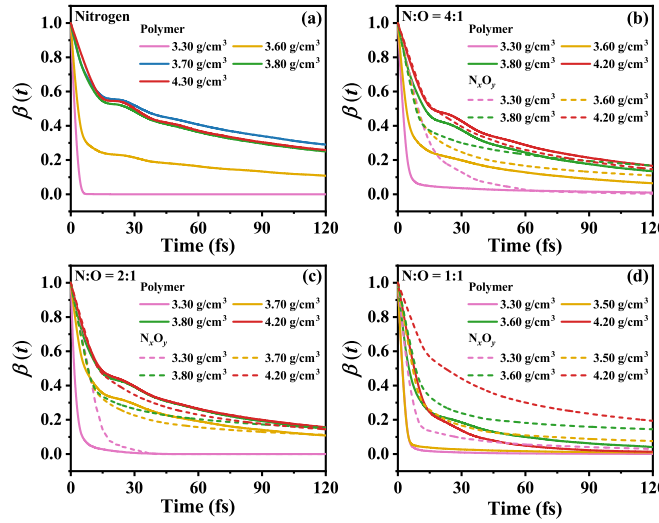

FIG. 4. Bond autocorrelation functions $\beta(t)$ for polymeric fluid and nitrogen oxides of N-O mixtures at representative cases along 2000 K.

to a polymeric fluid in the LLPT process, which agrees with previous works [16,17]. Features uncommon to liquid nitrogen are present in N-O mixtures. The $g(r)_{\text{N-N}}$ of N-O mixtures show the same trend as that of pure nitrogen. It is noted that oxygen molecules are almost completely dissociated during the phase transition, and a noticeable peak appears in the $g(r)_{\text{N-O}}$ at ∼1.24 Å, which indicates the new molecular states of nitrogen oxides (N_xO_y). The presence of oxygen gives rise to the chemical reaction as $N_2 + O_2 \rightleftharpoons N_xO_y$. Therefore, the LLPTs in N-O mixtures are associated with the transformation from molecular liquid to a mixed fluid of polymer and N_xO_y. Note that the N-O mixtures with different oxygen ratios show nearly the same structural properties in the LLPT process. This cannot explain the continuous weakening of the LLPT with an increasing oxygen concentration as reflected in isotherms and conductivities, which needs an exhaustive analysis.

The stability of the above-mentioned local structures can be illustrated by the bonding lifetime τ. Therefore, we calculate the bond autocorrelation function $\beta(t)$ of N-O mixtures so that τ can be estimated using two-exponentially-decay functions fit to $\beta(t)$ [62–67]. Detailed method descriptions are provided in the SM [52]. Figure 4 displays the calculated $\beta(t)$ for polymeric fluid and N_xO_y in N-O mixtures at conditions the same as in Fig. 3, and the resulting bond lifetimes τ are listed in Table I. The typical average vibrational periods [67] of N_2, O_2, and the nitrogen oxides are 12–16 fs. Under the molecular state (3.30 g/cm^3) before the transition, τ_{N_2} and τ_{O_2} are maintained for 6–11 times their average vibrational period. For pure nitrogen, the stable polymeric state possesses a long lifetime beyond 100 fs in the LLPT process. With an increased oxygen participation, the lifetime of the polymeric structure τ_{poly} is gradually shortened to 15.5 fs for N:O = 1:1, whereas that for nitrogen oxides $\tau_{N_xO_y}$ continues to increase to approximately 90 fs. The dissociation and recombination of N_2 and O_2 molecules, and the formation of N_xO_y products for N:O = 1:1 were also suggested by Jiang *et al.* [22], though their *P*-*T* conditions along the Hugoniot are much high than the present LLPT range. These imply that, in the N-O mixtures with more oxygen, the system is composed of more stable nitrogen oxides and the short-lived polymeric structure in the LLPT process, which thereby results in a weakened LLPT. Above all, it can be inferred that the LLPTs in N-O mixtures are dominated primarily by the molecular to polymeric transformation, and the participation of oxygen weakens the LLPT by promoting chemical reactions with nitrogen and crippling the polymerizations. The inherent structures in the LLPT process are illustrated intuitively from the charge density isosurfaces of the system, as seen in Fig. S7 [52].

TABLE I. Bond lifetimes (τ) of N-O mixtures at representative density (ρ) along the 2000-K isotherms, including N_2 (τ_{N_2}), O_2 (τ_{O_2}), polymeric fluid (τ_{poly}), and nitrogen oxides N_xO_y ($\tau_{N_xO_y}$). The lowest and highest ρ are before and after the first-order LLPT, respectively, and the adjacent ρ expresses the coexistence region.

	Nitrogen					N:O = 4:1				N:O = 2:1				N:O = 1:1			
ρ(g/cm^3)	3.30	3.60	3.70	3.80	4.30	3.30	3.60	3.80	4.20	3.30	3.70	3.80	4.20	3.30	3.50	3.60	4.20
τ_{N_2}	109.8	74.3	66.1	58.1	5.4	94.0	76.1	49.3	8.3	98.8	53.8	28.7	20.5	126.2	113.6	132.6	4.1
τ_{O_2}						110	37.4	0.0	0.0	90.2	21.6	9.0	0.0	109.1	61.3	32.3	0.0
τ_{poly}	2.0	39.2	119.8	106.5	118.4	3.0	26.2	74.9	67.9	2.9	43.3	59.2	61.7	2.5	2.6	20.9	15.5
$\tau_{N_xO_y}$						15.2	47.9	80.0	64.1	9.3	98.9	94.2	80.3	14.5	50.5	86.7	93.5

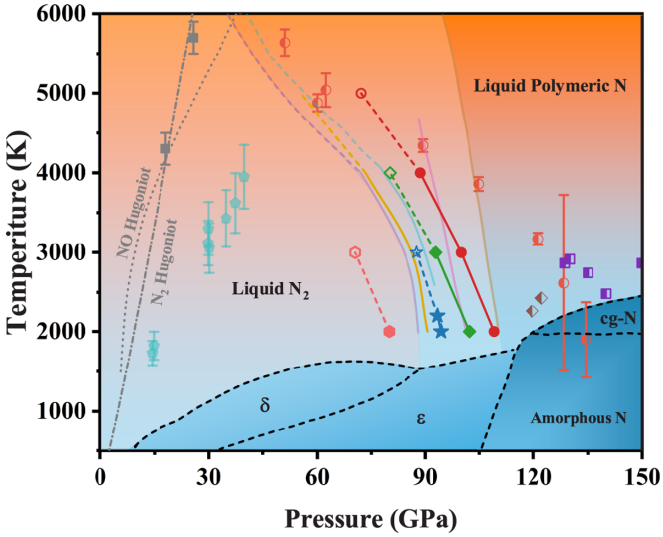

FIG. 5. The LLPT boundaries of N-O mixtures are depicted in the phase diagram for nitrogen. Current computed transition points and solid connected lines are determined from discontinuities of the isotherms, structure, and transport properties, while the extended dashes and open points are the points where the polymer fluid or nitrogen oxides survive at least two vibrational periods. (PBE level: Yellow line for liquid nitrogen; SCAN-*r*VV10 level: Claret circle for liquid nitrogen; green diamond, blue pentagram, and orange hexagon for N-O mixtures at 4:1, 2:1, and 1:1, respectively). Synchrotron x-ray diffraction [30] record the crystallization of cubic gauche cg-N (brown half diamond) and laser heating experiments [31] for the onset of the absorptive and metallic states of the polymeric fluid nitrogen (orange semicircles and violet half square). Previous PBE [16,68] (light violet and light cyan lines, respectively), SCAN [17] (light pink line), and chemical model results [26] (light yellowish-brown line) for pure nitrogen are given for comparison. The principal Hugoniot of nitrogen as observed experimentally [27] (solid gray square), and predicted assuming chemical dissociation [69] (gray dashed-dotted line); multiple shocked experimental Hugoniots of nitrogen [70] (solid cyan pentagon), and NO Hugoniot based on density functional theory (DFT) [71] (gray dotted line). The lower dashed black curves displays melting curve and solid-state phase boundaries for pure nitrogen [28–31,61,68,72,73].

Figure 5 illustrates the phase diagram of nitrogen, together with the considered LLPT boundaries of nitrogen and N-O mixtures. The LLPT transition pressures are determined from the discontinuities of the isotherms and the physical properties aforementioned in Fig. 2. There exist critical points on the LLPT boundaries for all N-O mixtures. Above the LLPT critical point, the structural transition processes occur smoothly in the *P*-*T* phase diagram [16,17]. Therefore, the extended dashed lines with hollow points are estimated based on the fact that τ_{poly} or $\tau_{N_xO_y}$ are conserved for at least two vibrational periods [67]. The first-order LLPT of liquid nitrogen from the considered PBE functional is broadly consistent with that predicted by Boates *et al.* [16]. Compared with SCAN [17], the boundary line of liquid nitrogen by SCAN-*r*VV10 shifts approximately 7 GPa towards high pressures. The current SCAN-*r*VV10 results show that polymer fluid performed up to 109 GPa above the melting line, which improves the agreement with the synchrotron x-ray diffraction [30] and laser heating experiments [31]. This illustrates that the vdW interactions play a key role in the LLPT of nitrogen. Therefore, more effective approaches for the vdW effects may be a potential way to further improve the descriptions of LLPT. The phase transition pressure shifts to lower pressures as the oxygen ratio increases when at the same temperature. In particular, the phase boundaries of the N-O mixtures are narrowed with increasing oxygen ratio, which corresponds to a decreased critical temperature. For example, the critical temperature is $4000 < T_c < 5000$ K in pure nitrogen but drops to $2000 < T_c < 3000$ K in N:O = 1:1. The first-order LLPT becomes more inexplicit due to the influence of oxygen doping on the structure evolution process. The single shock Hugoniot of N_2 and NO by dynamic experiments and theoretical calculations are far away from the LLPT range [27,69,71]. Compared with the single shock, the multiple shocked experiments [70] can reach a lower T and higher P condition, which may provide a potential experimental pathway for the first-order LLPT. Our current phase boundaries not only reveal the LLPT blueprint of N-O mixtures but also provide a basis for future experimental research of binary mixture systems.

IV. CONCLUSIONS

We perform extensive AIMD simulations to explore the first-order LLPT of N-O mixtures under high pressures and temperatures. The SCAN-*r*VV10 function is used to improve the description for the short- to long-range vdW interactions. The LLPTs of N-O mixtures are determined by identifying the discontinuities on the pressure isotherms. The first-order LLPT of N-O mixtures coincides with a nonmetal-metal transition indicated by the significantly increased conductivity properties. Further structural analyses through pair correlation functions suggest that the participation of oxygen introduces chemical reactions with nitrogen, and the LLPTs in N-O mixtures are associated with the transformation from molecular liquid to a mixed fluid of polymeric fluid and nitrogen oxides. Moreover, the lifetime calculations reveal that a greater oxygen concentration results in more stable nitrogen oxides and short-lived polymeric structures, which weakens the LLPT. Finally, the LLPT phase boundaries for N-O mixtures are drawn, which may provide guidance for future experimental research.

ACKNOWLEDGMENTS

This work is supported by the National Natural Science Foundation of China (Grants No. 11802280, No. 11674292, No. 11872057, No. 12074274, and No. 11804037), the Science Challenge Project (Grant No. TZ2016001), the NSAF (Grant No. U1830101), and the Foundation and Frontier Research Project of Chongqing (No. cstc2018jcyjAX0348). We also acknowledge the support for the computational resources by the TianHe-2 in the LvLiang Cloud Computing Center of China.

[1] L. Henry, M. Mezouar, G. Garbarino, D. Sifre, G. Weck, and F. Datchi, Nature (London) **584**, 382 (2020).

[2] K. Takae and H. Tanaka, Proc. Natl. Acad. Sci. USA **117**, 4471 (2020).

[3] H. Tanaka, R. Kurita, and H. Mataki, Phys. Rev. Lett. **92**, 025701 (2004).

[4] N. Jakse and A. Pasturel, Phys. Rev. Lett. **99**, 205702 (2007).

[5] P. Ganesh and M. Widom, Phys. Rev. Lett. **102**, 075701 (2009).

[6] M. W. C. Dharma-wardana, D. D. Klug, and R. C. Remsing, Phys. Rev. Lett. **125**, 075702 (2020).

[7] S. Scandolo, Proc. Natl. Acad. Sci. USA **100**, 3051 (2003).

[8] G. Mazzola and S. Sorella, Phys. Rev. Lett. **114**, 105701 (2015).

[9] G. Mazzola, R. Helled, and S. Sorella, Phys. Rev. Lett. **120**, 025701 (2018).

[10] W. Lorenzen, B. Holst, and R. Redmer, Phys. Rev. B **82**, 195107 (2010).

[11] M. A. Morales, C. Pierleoni, E. Schwegler, and D. M. Ceperley, Proc. Natl. Acad. Sci. USA **107**, 12799 (2010).

[12] C. Pierleoni, M. A. Morales, G. Rillo, M. Holzmann, and D. M. Ceperley, Proc. Natl. Acad. Sci. USA **113**, 4953 (2016).

[13] C. Tian, F. Liu, H. Yuan, H. Chen, and A. Kuan, J. Chem. Phys. **150**, 204114 (2019).

[14] H. Y. Geng, Q. Wu, M. Marqués, and G. J. Ackland, Phys. Rev. B **100**, 134109 (2019).

[15] B. Cheng, G. Mazzola, C. J. Pickard, and M. Ceriotti, Nature (London) **585**, 217 (2020).

[16] B. Boates and S. A. Bonev, Phys. Rev. Lett. **102**, 015701 (2009).

[17] G. Zhao, H. Wang, M. C. Ding, X. G. Zhao, H. Y. Wang, and J. L. Yan, Phys. Rev. B **98**, 184205 (2018).

[18] B. Boates, A. M. Teweldeberhan, and S. A. Bonev, Proc. Natl. Acad. Sci. USA **109**, 14808 (2012).

[19] T. Guillot, Science **286**, 72 (1999).

[20] W. B. Hubbard, W. J. Nellis, A. C. Mitchell, N. C. Holmes, S. S. Limaye, and P. C. McCandless, Science **253**, 648 (1991).

[21] N. Nettelmann, K. Wang, J. J. Fortney, S. Hamel, S. Yellamilli, M. Bethkenhagen, and R. Redmer, Icarus **275**, 107 (2016).

[22] X. Jiang, G. Chen, X. Cheng, Y. Li, and F. Guo, J. Phys. Chem. C **120**, 13366 (2016).

[23] P. Cheng, X. Yang, X. Zhang, Y. Wang, S. Jiang, and A. F. Goncharov, J. Chem. Phys. **152**, 244502 (2020).

[24] Z. Fu, Q. Chen, Z. Li, J. Tang, W. Zhang, W. Quan, J. Li, J. Zheng, and Y. Gu, High Energy Density Phys. **31**, 52 (2019).

[25] J. G. Ojwang, R. S. McWilliams, X. Ke, and A. F. Goncharov, J. Chem. Phys. **137**, 064507 (2012).

[26] M. Ross and F. Rogers, Phys. Rev. B **74**, 024103 (2006).

[27] W. J. Nellis, H. B. Radousky, D. C. Hamilton, A. C. Mitchell, N. C. Holmes, K. B. Christianson, and M. van Thiel, J. Chem. Phys. **94**, 2244 (1991).

[28] D. Tomasino, Z. Jenei, W. Evans, and C. S. Yoo, J. Chem. Phys. **140**, 244510 (2014).

[29] A. F. Goncharov, J. C. Crowhurst, V. V. Struzhkin, and R. J. Hemley, Phys. Rev. Lett. **101**, 095502 (2008).

[30] G. Weck, F. Datchi, G. Garbarino, S. Ninet, J. A. Queyroux, T. Plisson, M. Mezouar, and P. Loubeyre, Phys. Rev. Lett. **119**, 235701 (2017).

[31] S. Jiang, N. Holtgrewe, S. S. Lobanov, F. Su, M. F. Mahmood, R. S. McWilliams, and A. F. Goncharov, Nat. Commun. **9**, 2624 (2018).

[32] J. Vorberger, I. Tamblyn, B. Militzer, and S. A. Bonev, Phys. Rev. B **75**, 024206 (2007).

[33] M. Schottler and R. Redmer, Phys. Rev. Lett. **120**, 115703 (2018).

[34] S. Aasland and P. F. McMillan, Nature (London) **369**, 633 (1994).

[35] S. Mikhail and D. A. Sverjensky, Nat. Geosci. **7**, 816 (2014).

[36] A. Burrows, W. B. Hubbard, J. I. Lunine, and J. Liebert, Rev. Mod. Phys. **73**, 719 (2001).

[37] N. Goldman and S. Bastea, J. Phys. Chem. A **118**, 2897 (2014).

[38] K. Lodders, Icarus **155**, 393 (2002).

[39] K. P. Driver, F. Soubiran, S. Zhang, and B. Militzer, J. Chem. Phys. **143**, 164507 (2015).

[40] Z. Fu, L. Jia, X. Long, J. Xia, X. Xiao, Y. Li, W. Zhang, and Z. Li, Phys. Plasmas **27**, 052701 (2020).

[41] H. Huang, Y. Fei, L. Cai, F. Jing, X. Hu, H. Xie, L. Zhang, and Z. Gong, Nature (London) **479**, 513 (2011).

[42] C. Wang and P. Zhang, J. Chem. Phys. **132**, 154307 (2010).

[43] B. Militzer, F. Gygi, and G. Galli, Phys. Rev. Lett. **91**, 265503 (2003).

[44] G. L. Schott, M. S. Shaw, and J. D. Johnson, J. Chem. Phys. **82**, 4264 (1985).

[45] G. Kresse and J. Furthmuller, Phys. Rev. B **54**, 11169 (1996).

[46] G. Kresse and D. Joubert, Phys. Rev. B **59**, 1758 (1999).

[47] J. P. Perdew, K. Burke, and M. Ernzerhof, Phys. Rev. Lett. **77**, 3865 (1996).

[48] H. Peng, Z.-H. Yang, J. P. Perdew, and J. Sun, Phys. Rev. X **6**, 041005 (2016).

[49] J. Sun, R. C. Remsing, Y. Zhang, Z. Sun, A. Ruzsinszky, H. Peng, Z. Yang, A. Paul, U. Waghmare, X. Wu, M. L. Klein, and J. P. Perdew, Nat. Chem. **8**, 831 (2016).

[50] N. D. Mermin, Phys. Rev. **137**, A1441 (1965).

[51] S. Nosé, J. Chem. Phys. **81**, 511 (1984).

[52] See Supplemental Material at http://link.aps.org/supplemental/10.1103/PhysRevB.103.144105 for results of convergence and finite-size effect, EOS of liquid N-O mixtures, neighbor length distribution correlation confidence C_{NLDC}, comparison between PBE and SCAN-*r*VV10 results, charge density isosurfaces, bond autocorrelation function $\beta(t)$ and bond lifetime τ, and time evolutions of energy and pressure.

[53] R. Kubo, J. Phys. Soc. Jpn. **12**, 570 (1957).

[54] D. A. Greenwood, Proc. Phys. Soc. **71**, 585 (1958).

[55] X. Gonze, B. Amadon, P. M. Anglade, J. M. Beuken, F. Bottin, P. Boulanger, F. Bruneval, D. Caliste, R. Caracas, M. Côté, T. Deutsch, L. Genovese, P. Ghosez, M. Giantomassi, S. Goedecker, D. R. Hamann, P. Hermet, F. Jollet, G. Jomard, S. Leroux *et al.*, Comput. Phys. Commun. **180**, 2582 (2009).

[56] Z. Q. Wang, Z. G. Li, Y. F. Wang, L. Liu, Y. J. Gu, Q. F. Chen, and X. R. Chen, Phys. Rev. E **100**, 033214 (2019).

[57] H. Sun, D. Kang, J. Dai, J. Zeng, and J. Yuan, Phys. Rev. E **89**, 022128 (2014).

[58] A. Kietzmann, B. Holst, R. Redmer, M. P. Desjarlais, and T. R. Mattsson, Phys. Rev. Lett. **98**, 190602 (2007).

[59] B. Boates and S. A. Bonev, Phys. Rev. B **83**, 174114 (2011).

[60] V. Labet, P. Gonzalez-Morelos, R. Hoffmann, and N. W. Ashcroft, J. Chem. Phys. **136**, 074501 (2012).

[61] D. Donadio, L. Spanu, I. Duchemin, F. Gygi, and G. Galli, Phys. Rev. B **82**, 020102(R) (2010).

[62] E. R. Meyer, C. Ticknor, M. Bethkenhagen, S. Hamel, R. Redmer, J. D. Kress, and L. A. Collins, J. Chem. Phys. **143**, 164513 (2015).

[63] R. Chau, S. Hamel, and W. J. Nellis, Nat. Commun. **2**, 203 (2011).
[64] R. J. Gowers and P. Carbone, J. Chem. Phys. **142**, 224907 (2015).
[65] L. Liu, Z. G. Li, J. Y. Dai, Q. F. Chen, and X. R. Chen, Phys. Rev. E **97**, 063204 (2018).
[66] G.-J. Guo, Y.-G. Zhang, K. Refson, and Y.-J. Zhao, Mol. Phys. **100**, 2617 (2002).
[67] K. P. Huber and G. Herzberg, *Molecular Spectra and Molecular Structure: IV. Constants of Diatomic Molecules* (Van Nostrand Reinhold, NewYork, 1979).
[68] K. P. Driver and B. Militzer, Phys. Rev. B **93**, 064101 (2016).
[69] Q.-F. Chen, L.-C. Cai, Y. Zhang, Y.-J. Gu, and F.-Q. Jing, J. Chem. Phys. **124**, 074510 (2006).
[70] D. Lacina and Y. M. Gupta, J. Chem. Phys. **141**, 084503 (2014).
[71] Y. Zhang, C. Wang, F. Zheng, and P. Zhang, J. Appl. Phys. **112**, 033501 (2012).
[72] D. A. Young, C. S. Zha, R. Boehler, J. Yen, M. Nicol, A. S. Zinn, D. Schiferl, S. Kinkead, R. C. Hanson, and D. A. Pinnick, Phys. Rev. B **35**, 5353 (1987).
[73] G. D. Mukherjee and R. Boehler, Phys. Rev. Lett. **99**, 225701 (2007).